Article

Application of an Arbitrary Lagrangian–Eulerian Method to Modelling the Machining of Rigid Polyurethane Foam

Zdenek Horak [1,*], Petr Tichy [2], Karel Dvorak [1] and Miloslav Vilimek [2]

[1] Department of Technical Studies, College of Polytechnics Jihlava, Tolsteho 16, 58601 Jihlava, Czech Republic; karel.dvorak@vspj.cz

[2] Department of Mechanics, Biomechanics and Mechatronics, Faculty of Mechanical Engineering, Czech Technical University in Prague, Technicka 4, 16607 Prague, Czech Republic; petr.tichy@fs.cvut.cz (P.T.); miloslav.vilimek@fs.cvut.cz (M.V.)

[*] Correspondence: zdenek.horak@vspj.cz; Tel.: +420-773-778-948

Abstract: Rigid polyurethane (PUR) foam, which has an extensive range of construction, engineering, and healthcare applications, is commonly used in technical practice. PUR foam is a brittle material, and its mechanical material properties are strongly dependent on temperature and strain rate. Our work aimed to create a robust FE model enabling the simulation of PUR foam machining and verify the results of FE simulations using the experiments' results. We created a complex FE model using the Arbitrary Lagrangian–Eulerian (ALE) method. In the developed FE model, a constitutive material model was used in which the dependence of the strain rate, damage initiation, damage propagation, and plastic deformation on temperature was implemented. To verify the FE analyses' results with experimentally measured data, we measured the maximum temperature during PUR foam drilling with different densities (10, 25, and 40 PCF) and at various cutting speeds. The FE models with a constant cutting speed of 500 mm/s and various PUR foam densities led to slightly higher T_{max} values, where the differences were 13.1% (10 PCF), 7.0% (25 PCF), and 10.0% (40 PCF). The same situation was observed for the simulation results related to various cutting speeds at a constant PUR foam density of 40 PCF, where the differences were 25.3% (133 mm/s), 10.1% (500 mm/s), and 15.5% (833 mm/s). The presented results show that the ALE method provides a good match with the experimental data and can be used for accurate simulation of rigid PUR foam machining.

Keywords: PUR foam; machining; finite element (FE) analyses; Arbitrary Lagrangian Eulerian

1. Introduction

Rigid polyurethane (PUR) foam has been successfully used in many industries [1,2] since 1937, when Otto Bayer first synthesised it [3]. PUR foam can be used with a wide range of moulds, and its mechanical properties can be varied, making it suitable for use in a wide range of applications. The structural stability and mechanical properties of PUR foam are highly dependent on several physical parameters. The most important factors influencing the mechanical properties of PUR foam are its temperature [4,5], the strain rate [6,7], exposure to UV radiation, and extent of oxidation [8,9]. All of these factors degrade its mechanical properties.

One common application of PUR foam is the development and testing of medical devices [10,11]. For this purpose, certified PUR foam (Sawbones, Vashon, WA, USA) with standardized structure and density are used. Hollensteiner [12] and Oroszlany [13] experimentally evaluated that the mechanical properties (e.g., modulus of elasticity and ultimate strength) of PUR foam are similar to those of bone tissue, thereby making PUR foam suitable for tests of medical devices. PUR foam as standardized material is optimal for testing; however, its thermomechanical properties differ completely from those of bone tissue, and whether PUR foam is ideal for testing instruments used in surgery (e.g., drills and mills) is uncertain.

The phenomenon of heat generation during machining is very complicated because it is influenced by numerous factors, including heat-induced changes in the properties of the machined material. The amount of heat increases primarily with increasing rate of plastic deformation during machining and increasing friction between the machined material and the tool. Arrazola [14] and others authors (e.g., [15,16]) have presented the results of numerical finite element (FE) simulations of machining, where heat generation and its effect on the machined material and the tool itself were modelled. However, all of these works have focused on the analysis of thermally stable metal materials.

To the best of our knowledge, no FE simulations of machining and analysis of heat generation during machining of PUR foam, which is a relatively thermally unstable material, have been reported. Therefore, this work aims to design and validate a suitable method of FE simulations for modeling PUR foam machining. The next aim was to experimentally measure the mechanical properties of PUR foam, defined as a temperature function, and to use these data as inputs for FE simulations. To validate the results realised for FE analyses simulating PUR foam machining, we used the maximum temperature on the tool's tip during machining. Therefore, the final aim was experimentally measurement of the maximal temperature during drilling into PUR foam for different cutting conditions.

2. Materials and Methods

2.1. Experimental Measurements of Material Properties of PUR Foam as a Function of Temperature

To carry out the analyses, we first experimentally measured the material properties of rigid PUR foam under both tension and compression at different temperatures so that these values could be used as input parameters for the FE simulations. To ensure similar conditions, experimental measurements and subsequent FE analyses were performed on PUR foam blocks (Sawbones, Vashon Island, WA, USA). Experimental measurements were realised on PUR foam samples with three density values—10, 25, and 40 PCF (Pounds per Cubic Foot) density in SI units 160.32, 400.46, and 640.74 kg/m^3. Tensile and compression tests were realised on the testing system ElectroPuls E10000 (Instron, Norwood, MA, USA) with a video extensometer when tests were realised in a controlled environment by the heating chamber. Tensile tests were realised on seven specimens for all analyzed PUR foam densities with specimen dimensions of $10 \times 10 \times 15$ mm. Compression tests were realised on five samples from each PUR foam density on samples $10 \times 10 \times 15$ mm under the same conditions as the tensile tests. The tested specimens were loaded by force until their destruction in temperature environments of 25, 90, and 155 °C. Both types of tests were load by a strain rate of 45 mm/min.

2.2. Experimental Measurement of Temperature on Tool's Tip during Drilling

One of the planned outputs of the FE analyses was the distribution of the heat on the cutting edge of the tool. For this reason, a series of experimental measurements were carried out to determine the maximum temperature at the tip of the drill when drilling into PUR foams with different densities. Experimental measurements were performed on PUR foam samples with a density of 10, 25, or 40 PCF, where the sample dimensions were $15 \times 15 \times 10$ mm. The drilling was performed with a dental drilling machine SI 923 Implantmed (W & H Dentalwerk GmbH, Laufen, Germany) on a 2.9 mm diameter drill BioniQ (LASAK Ltd., Prague, Czech Republic) with a cutting speed of 800, 3000, or 5000 rpm and an axial speed of 10, 30, or 45 mm/min, respectively. Seven samples were measured for each combination of density and cutting speed. The maximum temperature T_{max} on the drill bit was measured using an IR camera FLIR E40 (FLIR Systems Inc., Wilsonville, OR, USA), at the time the drill passed through the drill sample (see Figure 1). No coolant was used to cool the drill during the experiment.
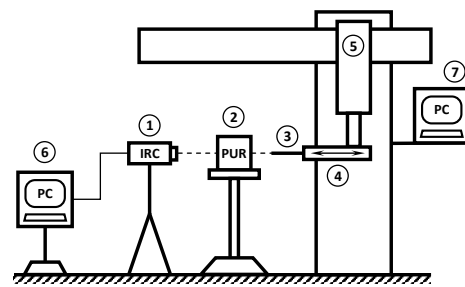
Figure 1. Experimental setup: 1—IR camera with connection to PC; 2—block of PUR foam; 3—drill; 4—dental drilling machine; 5—CNC milling machine with horizontal movement; 6 and 7—PC for drill movement controlling and recording data from IR camera.
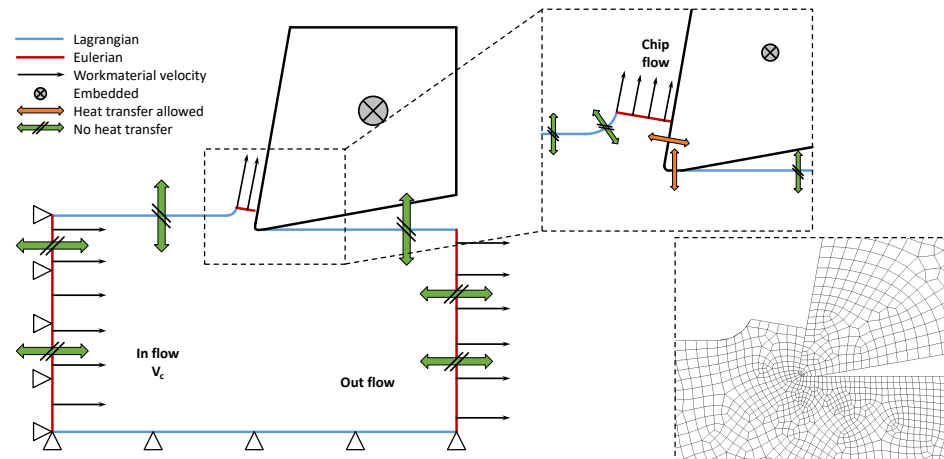
2.3. FE Simulation of the Machining

In this study, FE simulations of PUR foam machining of various densities and cutting speeds were performed. PUR foams are dependent on the crosslinking of the polymer chains [17]. However, in our work, PUR foam was modeled in the performed FE analyses as a material with global material properties defined by stress–strain dependencies. The stress–strain description of the material already includes the influence of the material's structure and character on a micro or molecular level. The PUR foam specimens were machined using a tool with edge roundness $r = 0.03$ mm, a 10° rake angle, and 10° clearance angles. The chip thickness was constant $t = 0.2$ mm, and the cutting speed vc was 133, 500, and 833 mm/s for all three PUR foam densities, corresponding to the drill speed (800, 3000, and 5000 rpm, respectively) used in the experiments.

PUR foam machining simulations were realised as a 2D task using the ALE formulation in ABAQUS/Explicit. ALE is a method that uses quality mesh throughout an analysis, even in case of large deformations or material damage, when the mesh is deformed independently of the material. Coupled thermal-stress analysis was used to affect temperature, where the output is the distribution of the temperature field in the machined material and cutting tool. During machining, the cutting edge of the tool compresses the workpiece and deforms via elastic and plastic deformation. The work associated with plastic deformation is transformed into heat. In the cutting plane, the chip shifts under high pressure, which is accompanied by considerable friction, and the chip is then rubbed across the face of the tool. Behind the cutting edge, because of the elastic component of the deformation, the material is pushed towards the back surface, and friction occurs again. Friction always results in the conversion of mechanical energy into heat. The heat is conducted to the chip, tool, and workpiece and is radiated to the surroundings. In the ALE model, heat transfer is only allowed on surfaces where contact occurred between the tool and the PUR foam.

In our study, the inflow and outflow surfaces of the model corresponded to Eulerian surfaces, including two outflow surfaces: the vertical surface of the workpiece and the surface on the top of the chip. The remaining surfaces were defined as Lagrangian surfaces. On the inflow surface, the node displacement was constrained in the horizontal direction, and the velocity of the material was equal to the cutting speed v_c. Bottom Lagrangian surfaces were constrained to be fixed in the vertical direction. The cutting tool was defined as the rigid body where a reference point was embedded (see Figure 2). Heat transfer was not allowed in any of the remaining areas (see Figure 2). The contact between the tool and the material was modelled as normal, which enabled separation after contact with a constant friction coefficient $f = 0.15$. Conductive heat transfer, defined by conductance k [W/(m·K)] as a function of closure c, was allowed. In actual FE analyses, the linear function of conductance $k = 0.01$ for $c = 0$ and $k = 0$ for $c = 10$ was used. The friction of the contact surfaces dissipates the energy that was completely converted into heat in our model when the heat was distributed equally between the two surfaces. An initial condition, temperature $T_0 = 293$ K, was applied throughout the model. In all of the realised fully coupled thermal-stress analyses, we specified an inelastic heat fraction to provide for inelastic energy dissipation as a heat source. Inelastic heat fractions were used for

large inelastic strain simulations, where the material deformation depends on the material properties influenced by heating. The value of inelastic heat fractions was set to 0.8 in all of the simulations.

Figure 2. Description of the Arbitrary Lagrangian–Eulerian model and detail of the mesh.

In the FE simulations, four-node bilinear plane strain thermally coupled quadrilateral elements with bilinear displacement and temperature, reduced integration were used. The global element size was 0.2 mm when contact surfaces were refined to the element size of 0.01 mm. Rigid PUR foam was modelled as a thermoelasto-viscoplastic material [18]. The elastic region of the material model was defined as temperature-dependent when the material properties were experimentally measured (see Section 3.1).

The selected material parameters are listed in Table 1. The Johnson–Cook material model was utilised; its flow stress is dependent on strain, strain rate, and temperature [19–21]. In Johnson–Cook hardening (adapted from [22]), the static yield stress is defined as

$$\overline{\sigma} = \left[A + B\left(\overline{\varepsilon}^{pl} \right)^n \right] \left[1 + C \, ln\left(\frac{\dot{\overline{\varepsilon}}^{pl}}{\dot{\varepsilon}_0} \right) \right] \left[1 - \Theta^m \right] \tag{1}$$

where A is the yield strength, B is the hardening modulus, C is the coefficient of strain rate sensitivity, n is the hardening coefficient, m is the thermal softening coefficient, $\Theta = (T - T_0)/(T_m - T_0)$ where T_0 is the transition temperature and T_m is the melting temperature, $\overline{\varepsilon}^{pl}$ is the Mises equivalent plastic strain, $\dot{\overline{\varepsilon}}^{pl}$ is the Mises equivalent plastic strain rate, and $\dot{\varepsilon}_0$ is the reference strain rate [23,24]. Used material constants were obtained from experimental measurements on PUR foam. (see Table 2).

The fracture model used for ductile materials consists of two phases: a damage-initiation phase and a damage-evolution phase. The primary mechanism that causes the ductile fracture of a ductile material is the nucleation, growth, and coalescence of voids. The ductile criterion is a model for predicting material damage when equivalent plastic strain is defined as a function strain rate and stress triaxiality

$$\overline{\varepsilon}_D^{pl}\left(\eta, \dot{\varepsilon}^{pl} \right) \tag{2}$$

where $\eta = -p/q$ is the stress triaxiality, p is the pressure stress, and q is the Mises equivalent stress (adapted from [22]). The damage initiation criterion was met when the following was applied:

$$\omega_D = \int \frac{d\overline{\varepsilon}^{pl}}{\overline{\varepsilon}_D^{pl}\left(\eta, \dot{\varepsilon}^{pl} \right)} = 1 \tag{3}$$

where ω_D is a state variable that increases together with plastic deformation (adapted from [22]). The incremental increase of ω_D is for each increment determined according to

$$\Delta\omega_D = \frac{\Delta\bar{\varepsilon}^{pl}}{\bar{\varepsilon}_D^{pl}\left(\eta, \dot{\varepsilon}^{pl}\right)} \geq 0. \tag{4}$$

Table 1. Material parameters of all PUR foams dependent on temperature.

	Equivalent Plastic Strain $\bar{\varepsilon}_D^{pl}$ [-]	Fracture Energy G_f [J/mm^2]	Density ρ [g/cm^3]	Specific Heat c_p [J/(kg.K)]	Conductivity k [J/(m.s.K)]
		40 PCF			
298.15 K	0.0400	40.0			
363.15 K	0.0290	29.0	0.64	809	0.11
428.15 K	0.2242	24.2			
		25 PCF			
298.15 K	0.0155	6.23			
363.15 K	0.0323	3.28	0.40	1 400	0.06
428.15 K	0.1494	2.60			
		10 PCF			
298.15 K	0.0315	0.866			
363.15 K	0.0421	0.245	0.16	1 477	0.037
428.15 K	0.2174	0.102			

Table 2. Johnson–Cook model parameters for rigid polyurethane foams with density of 10, 25 and 40 PCF.

Sample	A [MPa]	B [MPa]	n	C	$\dot{\varepsilon}_0$ [1/s]]	m	T_m [K]	T_0 [K]
10 PCF	1.4670	20.6235	0.831567	0.012	1	7.5052	675.0	273.15
25 PCF	4.3345	169.377	0.942053	0.012	1	11.623	675.0	273.15
40 PCF	11.9248	92.6822	0.686915	0.012	1	8.730	675.0	273.15

The value of equivalent plastic strain as a function of temperature for all PUR foams is given in Table 1. After the criteria for damage initiation have been established, the damage evolution must be set. For the damage evolution in ductile material, we modeled the stiffness decreasing until failure. Figure 3 presents a typical stress–strain curve for a material model with isotropic hardening until failure due to progressive specimen damage during a simple tensile test. The solid curve presented material model with damage and dashed curve material without damage.

In the graph in Figure 3, the yield stress σ_0, the equivalent plastic strain $\bar{\varepsilon}_0^{pl}$ and the equivalent plastic strain at failure $\bar{\varepsilon}_f^{pl}$. Upon reaching the damage initiation criterion, the damage variable increases by (adapted from [22])

$$\dot{d} = \frac{\dot{u}^{pl}}{\bar{u}_f^{pl}} \tag{5}$$

where $\bar{u}_f^{pl}$ is the equivalent plastic displacement at failure, defined by

$$\bar{u}_f^{pl} = \frac{2G_f}{\sigma_{y0}} \tag{6}$$

where σ_{y0} is the yield stress when the failure criterion is reached and G_f is the fracture energy.
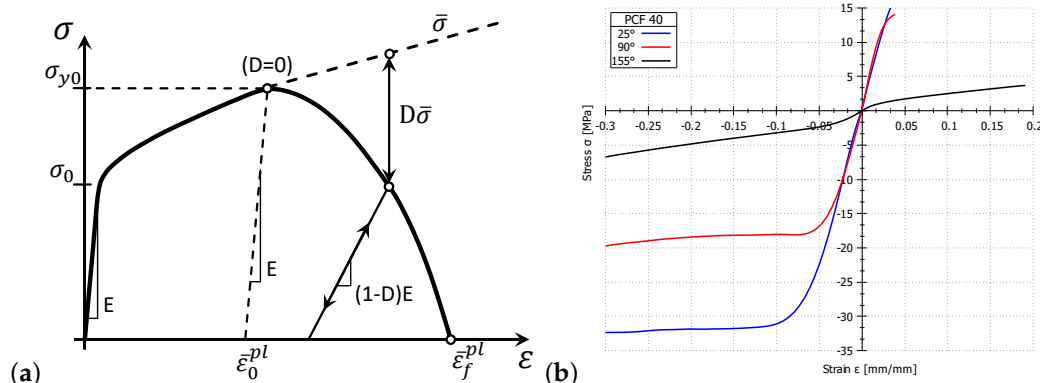
Figure 3. (**a**) Typical stress–strain curve for a material model with failure due to progressive damage simulated in Abaqus for specimen during a simple tensile test [22], (**b**) typical stress–strain curves for sample loaded by a 45 mm/min strain rate (40 PCF PUR foam).

3. Results

3.1. Material Properties of PUR Foam as a Function of Temperature

Experimental measurements were conducted to determine the temperature dependence of the mechanical properties of the PUR foams. The mean tensile and compressive modulus of the tested PUR foams with various densities, together with the mean size of tensile and compressive strength, were determined from experimental measurements. The typical stress–strain curve of the 40 PCF PUR foam is presented in Figure 3b for all three analysed temperatures (25, 90, and 155 Â °C). Results of the realised experimental measurement are presented in Table 3.

Table 3. Mechanical properties of PUR foams measured in experimental tests.

	25 °C		90 °C		155 °C	
Sample	**Tensile Modulus (MPa)**	**Compressive Modulus (MPa)**	**Tensile Modulus (MPa)**	**Compressive Modulus (MPa)**	**Tensile Modulus (MPa)**	**Compressive Modulus (MPa)**
PCF 10	86.25 ± 13.29	49.71 ± 9.94	53.07 ± 5.84	26.38 ± 4.75	3.01 ± 0.57	3.96 ± 0.52
PCF 25	309.06 ± 32.54	262.89 ± 55.21	280.32 ± 40.05	203.83 ± 20.38	8.48 ± 1.10	6.52 ± 0.59
PCF 40	543.95 ± 54.40	452.02 ± 94.92	507.19 ± 85.08	378.16 ± 41.31	71.29 ± 11.41	54.92 ± 9.89

### 3.2. Experimental Measurement of Heat on the Drill during Drilling

Experiments were conducted to determine the maximum temperature at the drill tip when drilling PUR foams of different densities at three cutting speeds (800, 3000, and 5000 rpm). Seven test samples were measured for each combination of density and cutting speed. The maximum temperature at the tip of the drill bit was measured using an infrared (IR) camera with a recording frequency of 10 Hz. The average value of the maximum temperature was obtained from the measured values. The results of the experimental measurements are summarised in Table 4. The results of experimental measurements of maximum temperature T_{max} show that the temperature at the drill bit increases with increasing density of the PUR foams and increasing cutting speed. Interestingly, the increase in T_{max} between the 10 PCF and 25 PCF materials is substantial: 74.3% for 800 rpm, 57.0% for 3000 rpm, and 67.1% for 5000 rpm. By contrast, the increase in T_{max} between the 25 PCF and 40 PCF materials was relatively small (32.3% for 800 rpm, 20.0% for 3000 rpm, and 16.9% for 5000 rpm).

Table 4. Experimentally measured maximum temperature T_{max} [°C] for three analysed revolution speeds and three PUR foam densities.

Rotation Speed [rpm]	800	3000	5000
Axial Speed [mm/min]	**10**	**30**	**45**
10 PCF	36.07 ± 2.3	61.90 ± 2.2	63.33 ± 4.4
25 PCF	62.87 ± 1.7	97.17 ± 5.2	105.80 ± 9.3
40 PCF	83.17 ± 1.2	116.63 ± 8.5	123.67 ± 9.5

*3.3. FE Simulation of the Machining*

The outputs of the FE analyses were the T_{max} at the tool cutting edge and the distribution of heat field in the rigid PUR foams with different densities (10, 25, and 40 PCF) during machining at various cutting speeds (133, 500, and 833 mm/s). The first parameter evaluated was the T_{max} at the tip of the cutting tool, which can be compared with experimentally measured values. The T_{max} values obtained from the FE analyses are given in Table 5 and Figure 4; the measured T_{max} values are reported in Table 4. The FE simulation results are in line with the expectation that with increasing temperature and cutting speed, the tool's tip and PUR foam temperature increase. Temperature distribution during machining of the PUR foam 40 PCF for various cutting speeds is presented in Figure 5.
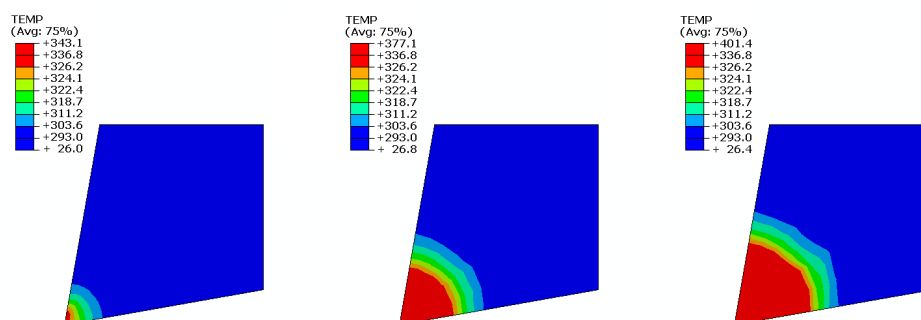
Figure 4. Temperature T [K] distribution on the tool's tip for constant cutting speed 500 mm/s during machining materials with different densities: 10 PCF (**left**), 25 PCF (**middle**), and 40 PCF (**right**).
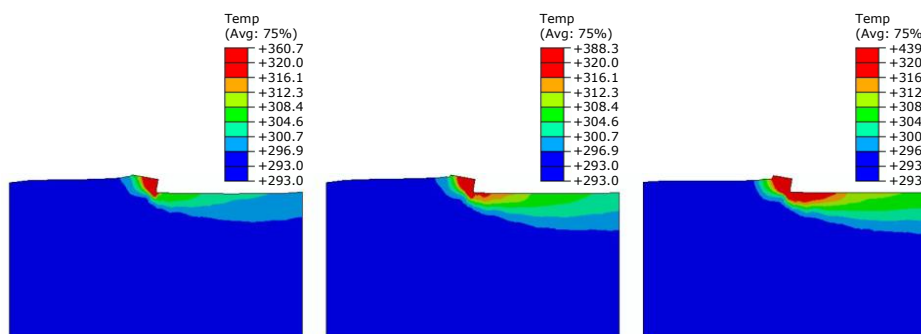
Figure 5. Temperature T [K] distribution during machining of the PUR foam with density 40 PCF : cutting speed 133 mm/s (**left**), 500 mm/s (**middle**), and 833 mm/s (**right**).

Table 5. Maximum temperature T$_{max}$ [°C] obtained from FE analyses for three analysed PUR foams with different densities (with constant cutting speed 500 mm/s) and various cutting speeds (with constant density of 40 PCF).

500 mm/s	10 PCF	25 PCF	40 PCF
T$_{max}$ [°C]	70.0	104.0	128.3
40 PCF	**133 mm/s**	**500 mm/s**	**833 mm/s**
T$_{max}$ [°C]	104.2	128.3	142.9

The second parameter evaluated was the temperature along two paths on the model. Path A started from the point of material contact with the cutting edge and proceeded towards the rear of the specimen. Path B started at the same position as Path A but was directed towards the centre of the rigid PUR foam (Figure 6).
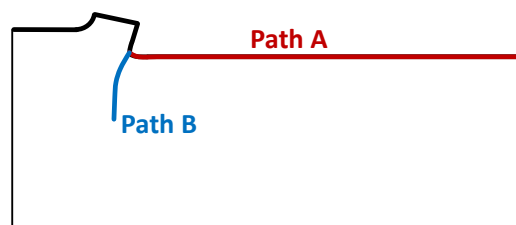
Figure 6. Schematic of Paths A and B on the model, where the temperature was analysed.

The values of the temperatures on both paths for evaluating the effect of the cutting speed on the model with a constant sample density (40 PCF) are shown in the graph in Figure 7a. On Path A, the temperature range for the cutting speed of 133 mm/s was in the range 121.8–35.0 °C, that for the speed of 500 mm/s was in the range 129.8–34.3 °C, and that for the speed of 833 mm/s was in the range 171.5–25.5 °C. On Path B, the temperature for the cutting speed of 133 mm/s was in the range 121.8–20.3 °C, that for the speed of 500 mm/s was in the range 129.8–20.0 °C, and that for the speed of 833 mm/s was in the range 171.5–9.2 °C. The temperatures on both paths for evaluating the effect of density on the model with a constant cutting speed (500 mm/s) are shown in Figure 7b. On Path A, the temperature for the 10 PCF sample was in the range 81.4–26.9 °C, that for the 25 PCF sample was in the range 109.4–30.1 °C, and that for the 40 PCF sample was in the range 129.8–34.3 °C. On Path B, the temperature for the 10 PCF sample was in the range 81.4–20.4 °C, that for the 25 PCF sample was in the range 109.4–21.0 °C, and that for the 40 PCF sample was in the range 129.8–20.0 °C.
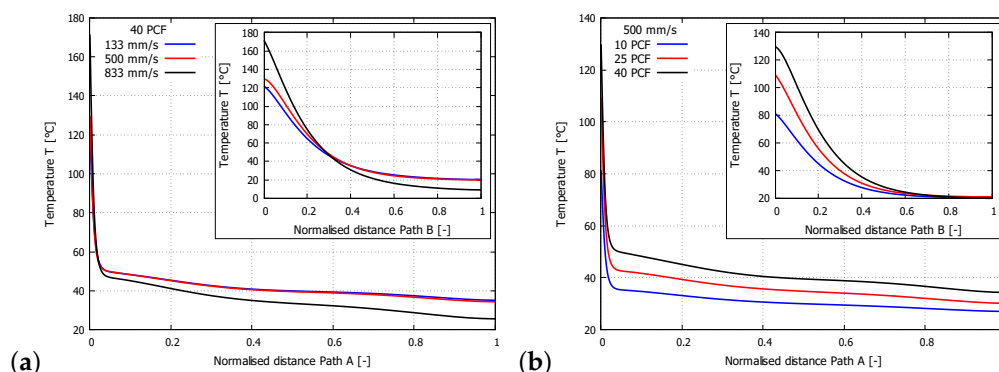
Figure 7. (**a**) Graph of the magnitude of the temperatures on Paths A and B for a constant density (40 PCF) with different cutting speeds. (**b**) Graph of the magnitude of the temperatures on Paths A and B for a constant cutting speed (500 mm/s) with different sample densities.

4. Discussion

The process of machining PUR foam was simulated by means of FEM as orthogonal cutting. Validation of the results from FE simulations was realised using experimentally measured data obtained from drilling into PUR foam. Although these types of machining are different, data can be compared with each other. In FE simulations, the orthogonal model's cutting speed was the same as the real drilling speed. Likewise, the cutting tool's dimensions (contact area) in the FE simulation were identical to those in the experimental drilling measurements. The used ALE method does not carry out the physical removal of material or generate chips during machining. Therefore the difference between the chip formation process during orthogonal machining and drilling is not relevant. The analysis's main goal was to determine the temperature at the tip of the tool, where heat generation depends on the cutting speed, the shape of the tool, and the physical conditions for heat conduction between the material and the tool. All the above parameters were the same for FE simulations and experimental measurements, and therefore, in our opinion, it is possible to compare the results of FE simulations and experimental measurements.

One factor that influenced the FE simulation results was the strain rate. Experimental measurements of PUR foam material parameters were performed at a cutting speed of 45 mm/min; however, in the FE simulations, the cutting speed ranged from 133 to 833 mm/s. During machining, the material is deformed at a velocity substantially greater than the sample loading speed in the experimental measurements. The mechanical properties of the PUR foam are highly dependent on the rate of deformation [7]; thus, this effect cannot be neglected. More accurate (depending on the temperature and strain rate) material parameters than those we have measured experimentally have not been published elsewhere. Therefore, using more appropriate material data as input data for FE simulations was not feasible.

The main aim of this work was to carry out a numerical FE analysis of rigid PUR foam machining using the ALE method and to verify the results by comparison with the results of experiments. To assess the validity of the FE model, we conducted a more detailed analysis of its energy balance. The total energy E_T can be set from the energy balance in the system as

$$E_T = E_I + E_V + E_{FD} + E_{KE} + E_{IHE} - E_W - E_{HF} \qquad (7)$$

where E_I is the internal energy (total strain energy), E_V is the viscous dissipated energy, E_{FD} is the frictional dissipated energy, E_{KE} is the kinetic energy, E_{IHE} is the internal heat energy, E_W is the work done by external forces, and E_{HF} is the external heat energy through external fluxes (adapted from [22]). When the material is machined, the dominant component of the energy is converted into total strain energy E_I, and internal heat energy E_{IHE}. The graph in Figure 8a shows the magnitude of the total energy E_T, the total strain energy E_I and the internal heat energy E_{IHE}. The graphs show that the total energy of the system or the energy balance according to Equation (8) is very small. The internal heat energy E_{IHE} is greater than the total strain energy E_I. Total strain energy was set as

$$E_I = E_E + E_P + E_A + E_{DMD} \qquad (8)$$

where E_E is the elastic strain energy, E_P is the inelastic dissipated energy, E_A is the artificial strain energy associated with constraints used to remove singular modes, and E_{DMD} is the energy dissipated by damage (adapted from [22]). To verify that hourglassing was not a problem in the FE simulations, we evaluated the artificial strain energy E_A more closely. For control of hourglass deformation, artificial strain energy E_A by the accumulated artificial strain energy was used . Because energy is dissipated through plastic deformation, $E_f \gg E_E$ applies a comparison E_A to an energy quantity that includes the dissipated energy as well, as the E_E is most meaningful in this analysis (Figure 8b). E_A is approximately 10.3% of E_f, therefore hourglassing does not influence results.

Figure 9 shows the magnitude of the total strain energy E_I, internal heat energy E_{IH}, and frictional dissipated energy E_{FD}. The graph for PUR foam with a density of 40 PCF and constant cutting speed of 500 mm/s shows that most energy is dissipated into friction and that substantially less energy is dissipated into material deformation. Frictional dissipated energy E_{FD} was set as 31.9 mJ (10 PCF), 184.0 mJ (25 PCF), and 200.5 mJ (40 PCF) for a constant cutting speed of 500 m/s. From the results, E_{FD} is only somewhat dependent on the sample density: the increase in E_{FD} between densities of 10 and 25 PCF is 476.8%, whereas the increase in E_{FD} between densities of 25 and 40 PCFs is only 8.9%. The magnitude of frictional dissipated energy E_{FD} is substantially more dependent on the magnitude of the cutting speed. A frictional dissipated energy E_{FD} of 55.9 mJ, 200.5 mJ, and 238.3 mJ was found at cutting speeds of 133, 500, and 833 mm/s for the 40 PCF sample, representing E_{FD} increases of 258.7% at 500 mm/s and 118.7% at 833 mm/s, compared with the E_{FD} at 133 mm/s.

Another parameter suitable for evaluating the FE model is the temperature at the point of contact of the tool with the material and its decrease with increasing distance from the tool on the material surface (Path A) and towards the inside of the material (Path B). The temperature graph in Figure 7 shows that the FE model works very well. The temperature value decreases substantially with increasing distance from the tool, consistent with the experimental results. The proposed FE model is sensitive to changes in material density and cutting speed. On the basis of these results, the results obtained with the ALE method match the experimental data well and can be used to accurately simulate the machining of rigid PUR foam.
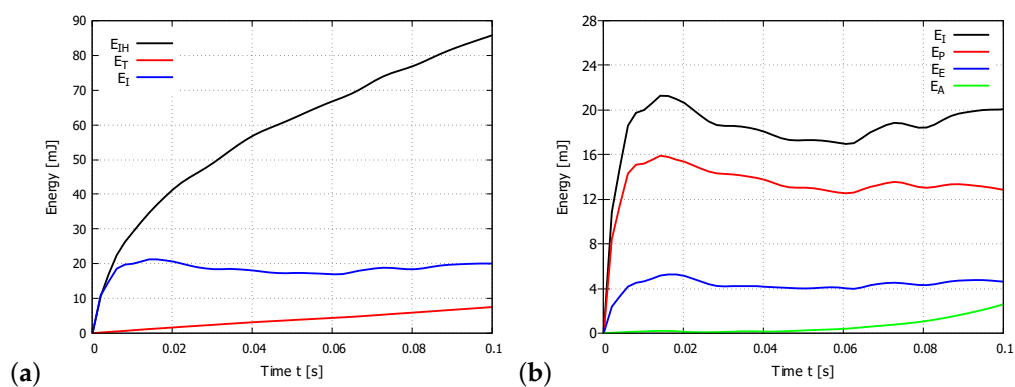
Figure 8. Graphs of energies in the FE model during cutting simulation (density 40 PCF): (**a**) internal heat energy E_{IHE}, total energy E_T, and total strain energy E_{EI}; (**b**) total strain energy E_I, inelastic dissipated energy E_P, elastic strain energy E_E, and artificial strain energy E_A.
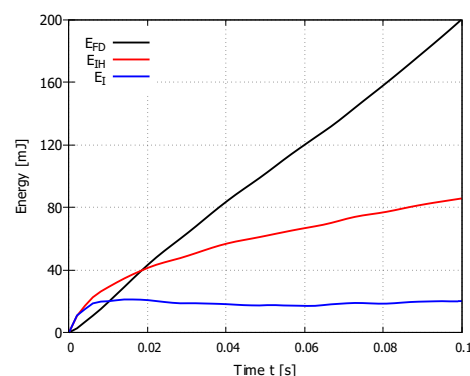
Figure 9. Graphs of frictional dissipated energy E_{FD}, internal heat energy E_{IH}, and total strain energy E_I in the FE model during a cutting simulation with constant cutting speed of 500 mm/s and a sample density 40 PCF.

Experimentally measured mechanical properties of rigid PUR foam were set as a function of the temperature when measurements were realised with specimens under both compression and tension. A total of seven samples were measured for each of the three PUR foam densities; this number appears to be statistically relevant because the measured data show a relatively low variance (13% or less).

The determination of the maximal temperature on the drill tip during drilling in PUR foams with different densities (10, 25 and 40 PCF) and various cutting speeds (800, 3000, and 5000 rpm) was performed experimentally.

For each combination of sample density and cutting speed, experimental measurements were performed on seven samples. This number appears to be statistically relevant because the measured data showed a relatively low variance (as high as 10%).

5. Conclusions

The main aim of this work was to carry out a numerical FE analysis of rigid PUR foam machining and to verify the results by comparison with the results of experiments. We created a complex FE model for simulating a brittle material machining, namely PUR foam, whose material properties are highly temperature-dependent. In the FE model, a unique complex constitutive material model was used in which the dependence of deformation rate, damage initiation, damage propagation, and plasticity on temperature was implemented. Such a complex material model used for deformation and heat propagation in a brittle material has not been presented anywhere yet. The Arbitrary Lagrangian–Eulerian method was used for FE machining simulations concerning minimal chip formation in brittle materials. In the realised FE simulations, the effect of various density and cutting speeds on the amount of heat generated during machining of the rigid PUR foam was evaluated.

Results obtained from FE analyses are in good agreement with the results of experimental measurements. The FE models with a constant cutting speed of 500 mm/s and various PUR foam densities led to slightly higher T_{max} values, where the differences were 13.1% (10 PCF), 7.0% (25 PCF), and 10.0% (40 PCF). The same situation is observed for the simulation results related to various cutting speeds at a constant PUR foam density of 40 PCF, where the differences were 25.3% (133 mm/s), 10.1% (500 mm/s), and 15.5% (833 mm/s). The results of FE analyses agreed well when the model sensitively responded to changes in the density of the PUR foam and the cutting speed. Upon closer evaluation of the FE model, we found that the internal heat energy was greater than the total strain energy, in agreement with the real situation. To verify that hourglassing was not a problem in the FE simulations, we evaluated the artificial strain energy; given that the artificial strain energy was 10.3% of the total internal energy, hourglassing was not a problem and the FE model was valid. According to the obtained results, the ALE method provides a good match with the experimental data and can be used to accurately simulate the machining of rigid PUR foams. The ALE method allows simulation of a long-term continuous machining process effectively without annoying restrictions such as computing cost and or excessive finite element distortions.

Experimentally measured mechanical properties of rigid PUR foam were set as a function of the temperature when measurements were realised with specimens under both compression and tension. An accurate description of the mechanical properties of PUR foam of different densities depending on temperature has not yet been published, and the relevance of the measured data for their use in the FE simulations is relatively high. From the results of the experimental measurements, it is clear that PUR foam is a specific material and cannot be modeled as a linear elastic material in numerical simulations.

The determination of the maximal temperature on the drill tip during drilling in PUR foams with different densities (10, 25, and 40 PCF) and various cutting speeds (800, 3000, and 5000 rpm) was performed experimentally. For each combination of sample density and cutting speed, experimental measurements were performed on seven samples. This number appears to be statistically relevant because the measured data showed a relatively low variance (as high as 10%). The results of the experimental measurements show that

the maximum temperature on the drill bit increases with increasing density of the PUR foam and increasing cutting speed. These results are in accordance with the predictions and were used only to verify the results of the FE analyses.

Author Contributions: Data curation, Z.H., K.D., and P.T.; Formal analysis, Z.H. and P.T.; Investigation, Z.H., K.D., M.V., and P.T.; Methodology, P.T.; Project administration, Z.H. and M.V.; Visualization, P.T. and Z.H.; Writing original draft, Z.H. and M.V. All authors have read and agreed to the published version of the manuscript.

Institutional Review Board Statement: Not applicable.

Informed Consent Statement: Not applicable.

Data Availability Statement: Not applicable.

Conflicts of Interest: The authors declare no conflict of interest.

Nomenclature

PUR	Rigid polyurethane foam
FEM	Finite element
ALE	Arbitrary Lagrangian–Eulerian
UV	Ultraviolet
PCF	Pounds per Cubic Foot
CNC	Computer Numeric Control
$\bar{\varepsilon}_D^{pl}$	Ductile equivalent plastic strain (-)
G_f	Fracture energy (J/mm^2)
ρ	Density (g/cm^3)
c_p	Specific heat (J/kg.K)
K	Conductivity (J/m.s.K)
IR	Infra red
T_{max}	Maximum temperature (K, °C)
v_R	Rotation cutting speed (rpm)
v_a	Axial cutting speed (mm/min)
t	Chip thickness (mm)
f	Friction coefficient (-)
k	Conductance (W/m.K)
$\bar{\sigma}$	Static yield stress (MPa)
A	Yeld strength (MPa)
B	Hardening modulus (MPa)
C	Coefficient of strain rate sensitivity (-)
n	Hardening coefficient (-)
m	Thermal softening coefficient (-)
T_0	Transition temperature (K)
T_m	Melting temperature (K)
$\bar{\varepsilon}^{pl}$	Mises equivalent plastic strain (-)
$\dot{\bar{\varepsilon}}^{pl}$	Mises equivalent plastic strain rate
$\dot{\varepsilon}_0$	Reference strain rate (1/s)
η	Stress triaxiality
p	Preasure stress (MPa)
q	Mises equivalent stress
ω_D	State variable
$\bar{\varepsilon}_0^{pl}$	Equivalent plastic strain (-)

$\bar{\varepsilon}_f^{pl}$	Equivalent plastic strin at failure (-)
$\bar{u}_f^{pl}$	Equivalent plastic displacement at failure (-)
E_T	Total energy (mJ)
E_I	Total strain energy (mJ)
E_V	Viscous dissipated energy (mJ)
E_{FD}	Frictional dissipated energy (mJ)
E_{KE}	Kinetic energy (mJ)
E_{IHE}	Internal heat energy (mJ)
E_W	Work done by external forces (mJ)
E_{HF}	External heat energy (mJ)
E_E	Elastic strain energy (mJ)
E_P	Inelastic dissipated energy (mJ)
E_A	Artificial strain energy (mJ)
E_{DMD}	Energy dissipated by damage (mJ)

References

1. Gama, N.; Ferreira, A.; Barros-Timmons, A. Polyurethane Foams: Past, Present, and Future. *Materials* **2018**, *11*, 1841. [CrossRef] [PubMed]
2. Harith, I.K. Study on polyurethane foamed concrete for use in structural applications. *Case Stud. Constr. Mater.* **2018**, *8*, 79–86. [CrossRef]
3. Ionescu, M. *Chemistry and Technology of Polyols for Polyurethanes*; iSmithers Rapra Publishing: Shrewsbury, UK, 2005.
4. Formela, K.; Hejna, A.; Zedler, L.; Przybysz, M.; Ryl, J.; Saeb, M.R.; Piszczyk, L. Structural, thermal and physico-mechanical properties of polyurethane brewers spent grain composite foams modified with ground tire rubber. *Ind. Crops Prod.* **2017**, *108*, 844–852. [CrossRef]
5. Zhang, M.; Pan, H.; Zhang, L.; Hu, L.; Zhou, Y. Study of the mechanical, thermal properties and flame retardancy of ofrigid polyurethane foams prepared from modified castor-oil-basedpolyols. *Ind. Crops Prod.* **2014**, *59*, 1595–1599. [CrossRef]
6. Chen, W.; Lu, F.; Winfree, N. High-strain-rate Compressive Behavior of a Rigid Polyurethane Foam with Various Densities. *Exp. Mech.* **2002**, *42*, 65–73. [CrossRef]
7. Mane, J.V.; Chandra, S.; Sharma, S.; Ali, H.; Chavan, V.M.; Manjunath, B.S.; Patel, R.J. Mechanical Property Evaluation of Polyurethane Foam under Quasi-static and Dynamic Strain Rates—An Experimental Study. *Procedia Eng.* **2017**, *173*, 726–731. [CrossRef]
8. Burgaz, E.; Kendirlioglu, C. Thermomechanical behavior and thermal stability of polyurethane rigid nanocomposite foams containing binary nanoparticle mixtures. *Polym. Test.* **2019**, *77*, 105930. [CrossRef]
9. Pellizzi, E.; Lattuati-Derieux, A.; Lavedrine, B.; Cheradame, H. Degradation of polyurethane ester foam artifacts: Chemical properties, mechanical properties and comparison between accelerated and natural degradation. *Polym. Degrad. Stab.* **2014**, *107*, 255–261. [CrossRef]
10. Er, M.S.; Altinel, L.; Eroglu, M.; Verim, O.; Demir, T.; Atmaca, H. Suture anchor fixation strength with or without augmentation in osteopenic and severely osteoporotic bones in rotator cuff repair: A biomechanical study on polyurethane foam model. *J. Orthop. Surg. Res.* **2014**, *48*, 247–253. [CrossRef] [PubMed]
11. Nowak, B. Experimental study on the loosening of pedicle screws implanted to synthetic bone vertebra models and under non-pull-out mechanical loads. *J. Mech. Behav. Biomed.* **2019**, *98*, 200–204. [CrossRef] [PubMed]
12. Hollensteiner, M.; Esterer, B.; Furst, D.; Schrempf, A.; Augat, P. Development of open-cell polyurethane-based bone surrogates for biomechanical testing of pedicle screws. *J. Mech. Behav. Biomed.* **2019**, *97*, 247–253. [CrossRef] [PubMed]
13. Oroszlany, A.; Nagy, P.; Kovacs, J.G. Compressive Properties of Commercially Available PVC Foams Intended for Use as Mechanical Models for Human Cancellous Bone. *Acta Polytech. Hung.* **2015**, *12*, 89–101.
14. Arrazola, P.J.; Ozel, T. Investigations on the effects of friction modeling in finite element simulation of machining. *Int. J. Mech. Sci.* **2010**, *52*, 31–42. [CrossRef]
15. Courbon, C.; Mabrouki, T.; Rech, J.; Mazuyer, D.; D'Eramo, E. On the existence of a thermal contact resistance at the tool-chip interface in dry cutting of AISI 1045: Formation mechanisms and influence on the cutting process. *Appl. Therm. Eng.* **2013**, *50*, 1311–1325. [CrossRef]
16. Pimenov, D.; Guzeev, V. Mathematical model of plowing forces to account for flank wear using FME modeling for orthogonal cutting scheme. *Int. J. Adv. Manuf. Technol.* **2017**, *89*, 3149–3159. [CrossRef]
17. Dhaliwal, G.; Anandan, S.; Chandrashekhara, K.; Lees, J.; Nam, P. Development and characterization of polyurethane foams with substitution of polyether polyol with soy-based polyol. *Eur. Polym. J.* **2018**, *107*, 105–117. [CrossRef]
18. Briody, C.; Duignan, B.; Jerrams, S.; Tiernan, S. The implementation of a visco-hyperelastic numerical material model for simulating the behaviour of polymer foam materials. *Comput. Mater. Sci.* **2012**, *64*, 47–51. [CrossRef]

19. Avevor, Y.; Vincent, J.; Faure, L.; Moufki, A.; Philippon, S. An ALE approach for the chip formation process in high speed machining with transient cutting conditions: Modeling and experimental validation. *Int. J. Mech. Sci.* **2017**, *130*, 546–557. [CrossRef]
20. Haglund, A.; Kishawy, H.; Rogers, R. An exploration of friction models for the chip-tool interface using an Arbitrary Lagrangian–Eulerian finite element model. *Wear* **2008**, *265*, 452–460. [CrossRef]
21. Johnson, G.; Cook, W. A constitutive model and data for metals subjected to large strains high strain rates and high temperatures. In Proceedings of the 7th International Symp. Balistics, Hague, The Netherlands, 19–21 April 1983.
22. ABAQUS Inc. *ABAQUS Analysis UserÂ's Manual, Version 2018*; ABAQUS Inc.: London, UK, 2018.
23. Ducobu, F.; Riviere-Lorphevre, E.; Filippi, E. Application of the Coupled Eulerian-Lagrangian (CEL) method to the modeling of orthogonal cutting. *Eur. J. Mech. A-Solid* **2016**, *59*, 58–66. [CrossRef]
24. Zetterberg, M. A Critical Overview of Machining Simulations in ABAQUS. Ph.D. Thesis, KTH Royal Institute of Technology, Stockholm, Sweden, 2014.